The Astrophysical Journal, 660:1541–1555, 2007 May 10

COLLISIONAL VAPORIZATION OF DUST AND PRODUCTION OF GAS IN THE β PICTORIS DUST DISK

A. Czechowski
Space Research Centre, Polish Academy of Sciences, PL 00-716 Warsaw, Poland; ace@cbk.waw.pl

and

I. Mann
Department of Earth and Planetary Sciences, Faculty of Science, Kobe University, Nada, Kobe 657-8501, Japan; mann@diamond.kobe-u.ac.jp
Received 2006 September 27; accepted 2007 January 18

ABSTRACT

The need for replenishment of the stable gas observed in the β Pictoris system raises a question about the origin of the gas. Correlations between the gas and the dust distribution suggest that the source is related to the dust. Spectroscopic observations imply that the gas is rotating at Keplerian velocity: this includes also the species that, in absence of braking, would be accelerated away from the star by the radiation pressure. We examine the possibility that the gas originates from collisional vaporization of the dust in the disk and the consequences for the gas velocity distribution and the line profiles of spectral features generated by the gas. A simple model of dust distribution and a model of individual dust-dust collision are used to calculate the gas production rate in the disk. Comparing with the gas column densities derived from observations, the escape times of the atoms from the disk are estimated. For the dust distribution and collision model considered, the vaporization of dust leads to the gas production rates of the order between 0.5×10^{12} and 2×10^{13} g s^{-1} for the grains with the collisional properties close to those of silicate and ice, respectively. We point out the uncertainties in the collision models. We also found that, for the lines of sight bypassing the star, velocity distributions of gas particles released from orbiting bodies can show a peak at Keplerian velocity even in the absence of braking, despite large acceleration by radiation pressure.

Subject headings: circumstellar matter — planetary systems: protoplanetary disks — stars: individual (β Pictoris)

1. INTRODUCTION

β Pictoris is surrounded by one of the best-studied circumstellar debris shells: a disklike accumulation of dust particles generated by larger planetesimals or comet-like objects possibly shaped by planets hidden within this disk. Among the circumstellar debris disks that were observed until today the case of β Pictoris is distinguished not only by high dust density (Backman & Paresce 1993) but also by the presence of a relatively high amount of circumstellar gas comprising a stable and a time-variable component (see Lagrange et al. 1995). Shortly after the discovery of the dust, observations indicated the presence of circumstellar gas initially inferred from the detection of Ca II and Na I (Hobbs et al. 1985). Further observations of the Ca II absorption showed a relatively stable narrow absorption feature combined with a time-variable component (see Ferlet et al. 1987; Vidal-Madjar et al. 1998). The majority of detected time-variable gas is seen with high redshift and interpreted as due to comet-like objects falling into the star (Beust et al. 1996, 1998; Beust & Morbidelli 2000). The sources of the gas components are still under discussion. Understanding the origin of different gas components in the β Pictoris system would be important also for the study of other circumstellar debris disks.

In the following we focus on the stable gas component. The stable gas component was studied by measurements of absorption lines (Lagrange et al. 1998) and emission lines offset from the star (Olofsson et al. 2001). Gas densities for the stable component that have been inferred from observations vary a lot. By investigating the effect of gas drag on the dynamics of the dust particles, Thébault & Augereau (2005) recently concluded that the hydrogen gas number density at 117 AU should not exceed 10^4 cm^{-3} and from that determined an upper limit on the total gas mass of about 0.4 Earth masses. The radial profile of the gas derived from emission observations between about 30 and 120 AU seems to closely follow that of the dust (Olofsson et al. 2001). Follow-up observations of emission lines (Brandeker et al. 2004) showed that faint signals of gas extend further inward and outward. Similar to the dust density, the gas distribution shows a change in the symmetry plane from the inner to the outer disk, although the extension from the midplane is significantly larger than that of the dust disk.

The gas velocities are remarkably similar for different species (Liseau 2003). In particular, the emission lines observed along the line of sight passing through the disk at a distance d from the star were found to show a Doppler shift corresponding to the Keplerian speed for the orbit of radius d (Olofsson et al. 2001; Brandeker et al. 2004). A puzzling feature is the lack of the signatures, in both the absorption and the emission spectra, of the radial outflow expected for the case of high-β (high radiation pressure–to–gravity ratio) species, which should be accelerated away from the star by the radiation pressure. Therefore, a braking mechanism by collisional friction with a stable gas component was suggested (Lagrange et al. 1998; Olofsson et al. 2001; Brandeker et al. 2004). The required densities of the stable gas would be in conflict with observations, at least if the braking gas were hydrogen (Brandeker et al. 2004). Fernández et al. (2006) proposed that Coulomb interaction between different ion species (which couple the high-β species to low-β ones and thus decrease the effective β) and between the ions and charged dust grains provides that braking. The latter mechanism becomes more effective for the case of high carbon abundance, and therefore recent observations by Roberge et al. (2006), showing high abundance of carbon in the gas disk, are particularly relevant.

The spatial correlation with the dust density, the existence of volatile elements in the gas, and the Keplerian velocity signatures in the emission spectra all point toward a connection between the dust and the stable gas component. Since the fate of dust in the different stages of circumstellar disk evolution depends critically on the gas content of the system (see, e.g., Takeuchi et al. 2005; Takeuchi & Artymowicz 2001), understanding the mechanisms of the gas generation from dust around β Pictoris might also be relevant for other systems. So far no mechanism to produce the gas from dust or from the planetesimals has achieved quantitative agreement with observed gas column densities. In particular, the dust sublimation was ruled out as a process to generate the stable gas component (Lagrange et al. 1998; Artymowicz 1997), while Lecavelier des Etangs et al. (2001) suggest that observed CO absorption arises from evaporation of planetesimals. Collisional vaporization was suggested as a process of gas production, but not further quantified (Liseau & Artymowicz 1998; Lagrange et al. 1998).

In this paper we concentrate on the possibility that the origin of the stable gas is the collisional vaporization of the dust grains in the β Pictoris disk and study the initial Doppler shifts along the line of sight that would be generated by such a gas component.

We first introduce a model of the dust distribution in the disk (§ 2) based on the model description of dust-dust collisions and observations of the optical thickness of the disk. This model is then used (in § 3) to calculate the vaporization rate of the dust grains, which can be compared to the previous estimations of gas production rate (Lagrange et al. 1998; Fernández et al. 2006). The total mass vaporization rate in the disk following from our model is of the order 0.5×10^{12} and 2×10^{13} g s^{-1} for the cases of grains with the collisional characteristics of the astronomical silicate and ice, respectively.

Assuming that the collisional vaporization of the dust provides the main source of the gas, we estimate the escape times from the disk required to explain the column densities of different gas species derived from observations. For the high-β species we find the escape times of the order of 10^{12} s (silicate) or 10^{10} s (ice). We also derive the density distribution of a high-β species (taking Ca II as a specific example) under assumption that no mechanisms are available to retain the gas in the disk (§ 4). In § 5 we consider other gas production processes related to dust: stellar wind impact mechanism and sputtering.

In § 6 we discuss the velocity distributions of gas particles along a line of sight passing through the disk, concentrating on the peak in this distribution at the velocity corresponding to Keplerian orbit tangent to the line of sight. In § 7 we summarize our results and discuss them in the context of physical parameters used in the calculations. The conclusions are given in § 8.

2. MODEL OF DUST DISTRIBUTION

Our initial assumptions are similar to those of Krivov et al. (2000). We consider two subpopulations of the grains in the disk: the grains in bound orbits, with the radiation pressure–to–gravity ratio below the blowout limit ($\beta < \frac{1}{2}$ for the grains in circular Keplerian orbits), and the "β-meteoroids," with β above the blowout limit, assumed to originate from fragments produced during collisions between the grains. For compact grains the boundary between the bound grains and the β-meteoroids in the β Pictoris disk corresponds to the grain size $a \sim 2$ μm, with the exact value depending on the grain material (Fig. 1). Note that for some cases (in Fig. 1, ice) also the very small grains have the β-value below the blowout limit: although these grains would not be blown away by radiation pressure, they may be ejected due to interaction with the magnetic field of the star (Mann et al. 2007).

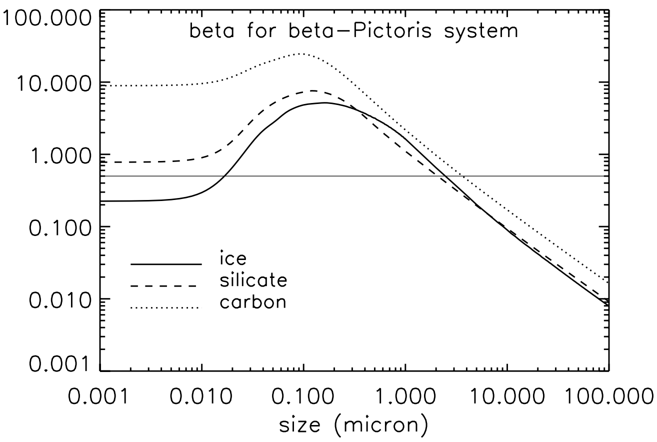

FIG. 1.—Radiation force–to–gravity ratio β as a function of size for dust grains in the β Pictoris system. The size range for which $\beta > 0.5$ (above the thin horizontal line) corresponds to β-meteoroids. The blackbody spectrum was assumed for the star (Köhler & Mann 2002).

The β-meteoroids we divide into generations. The zeroth generation consists of the β-meteoroids produced in collisions between the bound grains. The nth ($n > 0$) generation is produced by collisions between the ($n - 1$)-th generation β-meteoroids and the bound grains. Production of grains from the collisions between the β-meteoroids is not considered.

We assume the size distribution of the large grains in the disk at the distance r from the star to have the form

$$dn/da = C(r)a^{-3.5}, \quad (1)$$

where a is the grain radius and $C(r)$ is determined by the requirement that the geometrical cross section of the large-grain population accounts for the normal optical depth of the disk $\tau(r)$ at the distance r. We use the formula (Artymowicz & Clampin 1997)

$$\tau(r) = \frac{2\tau_m}{(r/r_m)^{-2} + (r/r_m)^2}, \quad (2)$$

where $r_m = 60$ AU and $\tau_m = 0.01$ (Krivov et al. 2000). This distribution is then used to calculate the production rate of fragments, with the fragments of size below the blowout limit interpreted as the zeroth generation β-meteoroids. The production rate and the distribution of nth generation β-meteoroids can be derived after the ($n - 1$)-th generation production rate is found. The average relative velocity of colliding large grains is calculated assuming that the bound grains are in circular orbits uniformly distributed in inclination within the disk (within 7° from the disk central plane). The effect of radiation pressure on the orbital velocity is taken into account; that is, the orbital velocities of the grains are dependent on the grain size. A detailed description of our model is given in Appendix A. Our description of an individual collision between the grains is based on that of Tielens et al. (1994). Figures 2 and 3 show the dependence of the vaporized and fragmented mass of the target grain per unit projectile mass assumed in the model.

The results are illustrated in Figures 4, 5, and 6. The size distributions, at the distance 100 AU from the star, of the bound grains and of the first four (eight for the carbon case) generations of the β-meteoroids are shown for the cases of grains with the optical (β) and mechanical (fragmentation parameters) properties of ice, astronomical silicate, and carbon. The case of carbon

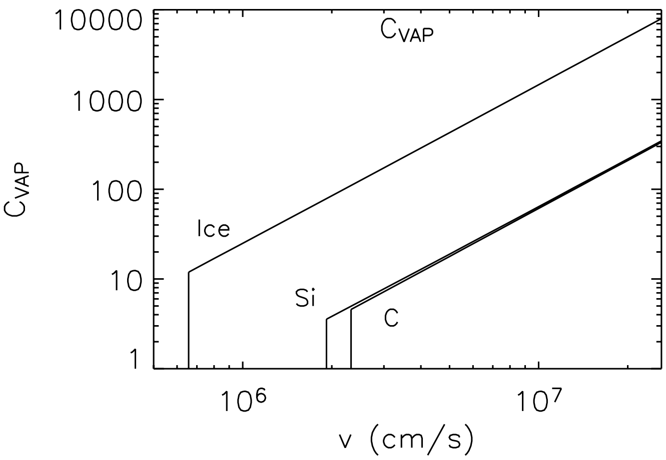

FIG. 2.—Vaporized mass of the target grain per unit projectile mass assumed in our collision model.

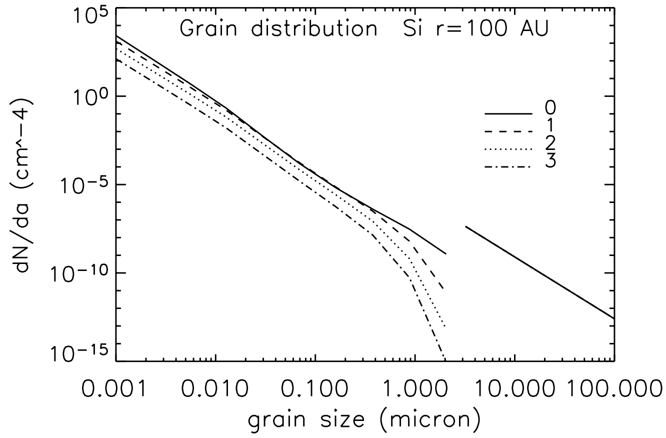

FIG. 4.—Example of grain size distributions assumed in our calculations: the distribution at the distance 100 AU from the star for the case of grains with the properties of silicate. For the sizes below the blowout limit, the contributions from different generations of the β-meteoroids ($n = 0$–3) are shown.

is the extreme one, with the small size part of the distribution dominated by high-generation particles. On the other hand, in the cases of ice and silicate grains the contributions from higher generations start diminishing after generation 1, suggesting that the higher orders ($n > 3$) can be neglected. The contributions from higher generations are smaller at smaller distances from the star: for example, at 50 AU the generations above $n = 4$ diminish with n even for the case of carbon. The role of the β-meteoroids in causing the vaporization of the larger grains is discussed in the next section.

The presence of higher generation β-meteoroids distinguishes our model from that of Krivov et al. (2000), who included only the zeroth generation. However, our model of an individual collision is different from that of Krivov et al. (2000); in particular, "cratering" events are included along with catastrophic collisions. We found that if only catastrophic collisions between the grains are included as in Krivov et al. (2000), the cascade of high-generation β-meteoroids is suppressed.

It should be noted that the presence of a large amount of β-meteoroids may contradict our assumption (based on observations) that the observed optical depth of the dust disk is determined by the bound grains. For example, at 100 AU from the star the grains in unbound orbits contribute 71% (silicate) and 39% (ice) of the dust geometrical cross section. However, their contributions to the scattering (extinction) cross sections that determine the optical depth are smaller: 8.4% (6.3%) for silicate and 8.6% (8.6%) for ice, for observations in visible light (wavelength 0.5 μm). The case of all carbon grains is different: the contribution of the $n = 0$–7 generations of β-meteoroids leads to 99.6% of the dust geometrical cross section and 93% (95%) of the scattering (extinction) cross section. Reducing the number density of bound carbon grains is not a solution: if the density everywhere in the disk is reduced by a factor of 2, the contribution of β-meteoroids decreases to 90% of the geometrical cross section and 39% (44%) of the scattering (extinction) cross section, so that the small carbon grains would still contribute significantly to the spectrum. Since the observations suggest that the scattering is dominated by the grains above the blowout size, the case of all carbon grains may therefore be in conflict with observations. Our estimations are based on Mie theory, assuming spherical grains of uniform composition.

Our model is chosen predominantly for its simplicity. It reproduces the optical thickness profile of the disk, but the details of the size distribution of large grains and the flux intensity of the β-meteoroids are not derived in a self-consistent way. It is known that the power-law $a^{-3.5}$ collisional distribution must be modified in the presence of the lower size cutoff (blowout limit in this case). The effect of collisions between the β-meteoroids and the larger grains on the distribution of bound grains, expected

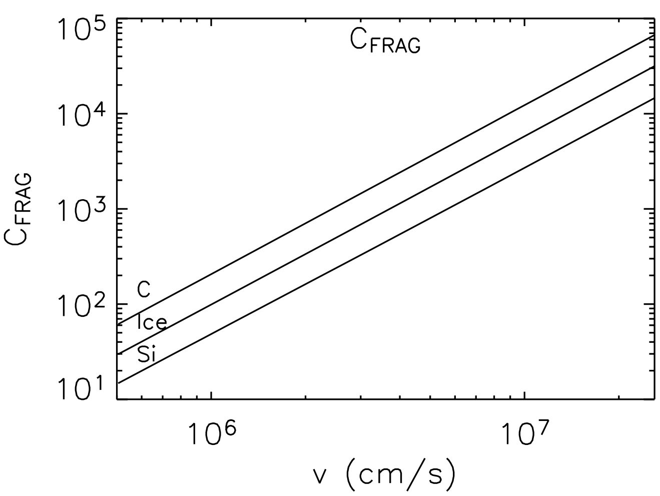

FIG. 3.—Fragmented mass of the target grain per unit projectile mass assumed in our collision model.

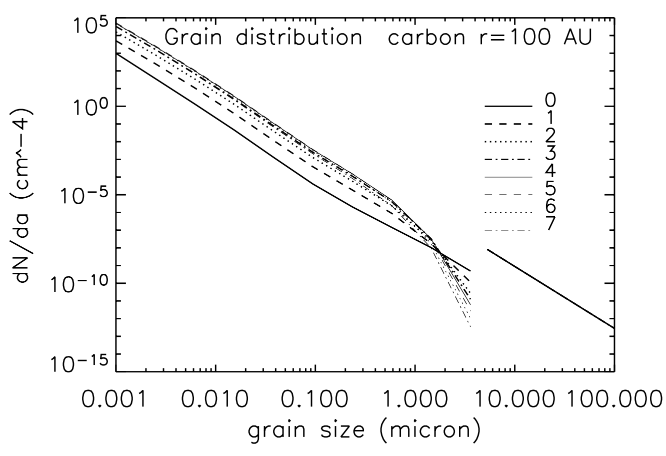

FIG. 5.—Same as Fig. 4, but for the case of carbon-type grains. The contributions from $n = 0$ to 7 generations are shown.

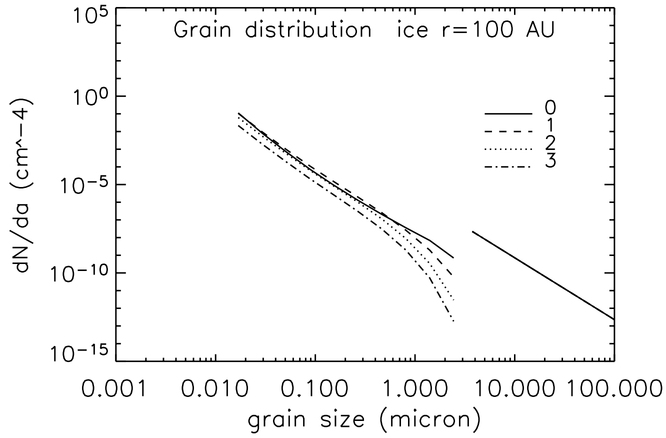

FIG. 6.—Same as Fig. 4, but for the grains with the properties of ice. In this case the grains with the sizes below $a = 0.015$ μm have $\beta < \frac{1}{2}$ and were not included in the calculations.

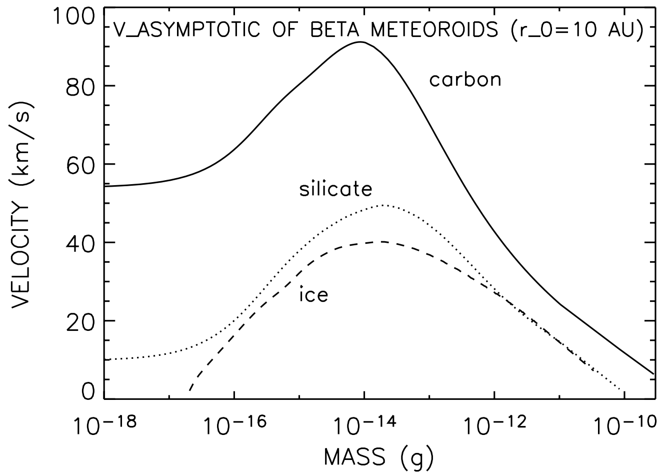

FIG. 7.—Asymptotic radial velocities v_∞ vs. mass for the β-meteoroids created at the distance $r_0 = 10$ AU from β Pictoris. For any other initial distance r the value of v_∞ is obtained by multiplication by the factor $(r/10 \text{ AU})^{-1/2}$.

to lead to the flattening of the size distribution near the blowout limit (Krivov et al. 2000), is not included in the model. We found, however, that if a pure power-law size distribution ($a^{-3.5}$) is replaced by a modified distribution with a reduced slope (a^0) for the sizes a within 1 order of magnitude from the blowout limit, the effect on the production of β-meteoroids and grain vaporization is not large. The reason is that the modified distribution must have the same geometrical cross section in order to fit the observed optical depth.

Another simplification is the assumption of circular orbit and uniform size distribution of the bound grains. Augereau et al. (2001) have presented a model in which the grains are created with an $a^{-3.5}$ size distribution but enter elongated orbits dependent on their value of β. This leads to the disk with position-dependent size distribution of the bound grains. We think, however, that in view of the uncertainties in the parameters of the model and in description of the individual collisions between the grains, the simplified model of the dust distribution assumed in our study can be regarded as adequate. Comparison between the gas production rates based on our model and that of Augereau et al. (2001) would require a detailed study. The main difference is in the velocity and spatial distribution of small bound grains, with the sizes close to the blowout limit. The effect of the grain size dependence of the orbital velocity is to some extent taken into account in our model. The fraction of small bound grains in the inner disk in the model of Augereau et al. (2001) is reduced. This implies, however, that the number density of larger grains in this region must be higher than in our model in order to produce the same optical thickness profile. Since a similar modification (see the previous paragraph) of our distribution of the bound grains did not lead to a substantial change in results, we expect that the difference between the two model predictions for dust vaporization rates will not be large.

3. COLLISIONAL VAPORIZATION OF GRAINS IN THE β PICTORIS DUST DISK

In a collision between dust grains the majority of the material lost to the target goes into fragments and only a small amount is vaporized (Figs. 2 and 3). Nevertheless, for the case of solar system dust, the vaporized part was found to contribute to the minor ions measured in the solar wind (Mann & Czechowski 2005).

Semiempirical models imply that even a partial vaporization of the dust material only occurs in the case when the relative velocity of the colliding grains is higher than a threshold velocity $v_{\rm th}$. The threshold velocity depends on the material and structure of the grains and is typically of the order of a few times 10 km s^{-1} (less for the case of ice), which is above the Keplerian velocity in most of the disk. As a result, except for the region very near the star, there would be no vaporization during collisions between the large-sized dust grains moving in Keplerian orbits. On the other hand, the small grains (β-meteoroids, $a \lesssim 2$ μm), for which radiation pressure dominates over the gravity, are not in bound orbits but stream through the disk at velocity increasing toward an asymptotic value and may initiate vaporization when striking a larger grain in a bound orbit. The vaporization rate is therefore determined by the collision rate between the grains belonging to two distinct populations. Figures 2 and 3 show the vaporized and fragmented mass of the target grain per unit projectile mass as a function of the collision velocity assumed in our calculations. These were derived using the formulae of Tielens et al. (1994). For threshold velocities for vaporization we use the values $v_{\rm th} = 6.5$ km s^{-1} (ice), 19.0 km s^{-1} (silicate), and 23.0 km s^{-1} (carbon) as given in Table 1 of Tielens et al. (1994). We note that by using these material parameters we do not intend to imply that they are representative of the elemental composition of the dust. This is further discussed in § 7.

The asymptotic radial velocity of a β-meteoroid can be expressed as $v_\infty(r_0) = [(2\beta - 1)GM/r_0]^{1/2} \equiv (2\beta - 1)^{1/2} v_{\rm orb}(r_0)$, where $v_{\rm orb}(r_0)$ is the Keplerian velocity at the distance r_0 where the β-meteoroid was created. Since β depends on the size of the grain, v_∞ is also size (mass) dependent. In Figure 7 we show the plots of v_∞ versus mass for grains of different composition for the same initial distance from the star $r_0 = 10$ AU. Note that the asymptotic speed is particularly high for the carbon grains. As a consequence, the carbon β-meteoroids will be the most effective in initiating vaporization of any target grains in this model of the β Pictoris dust disk. The β-meteoroids originating too far from the star will not, however, be able to attain the velocities above the vaporization threshold for carbon or silicate.

Figures 8, 9, and 10 show the calculated mass vaporization rate in the disk as a function of distance from the star for three sets of parameters describing the individual collision, corresponding to different choices of the grain material: ice, astronomical silicate, and carbon, with the same material assumed for the target and the projectile. In the region near the star, the dominant contribution comes from the collisions between the grains with the sizes above the blowout limit.

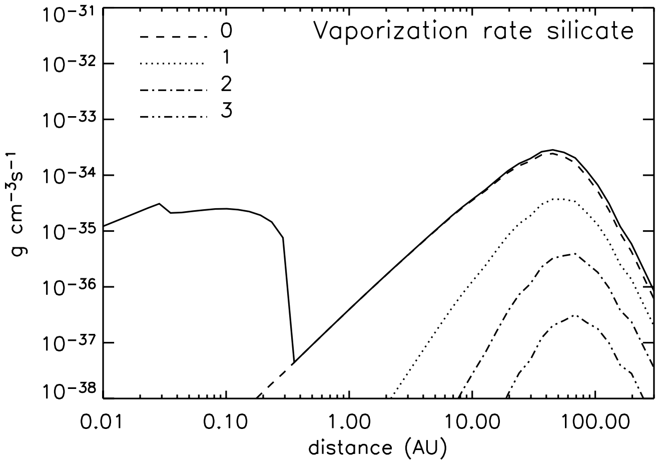

FIG. 8.—Calculated mass vaporization rate from dust collisions in the disk as a function of distance from the star assuming that the dust disk consists of the silicate-type grains. Collisions between the grains in the bound orbits ($\beta < 0.5$), as well as the collisions between the first four generations of β-meteoroids and the bound grains, are included. At larger distances only the collisions with β-meteoroids contribute to vaporization. Contributions from the impacts of different generations of β-meteoroids are shown besides the total contribution.

In our model the grains in bound orbits are assumed to move in circular orbits with orbital speed v dependent on the radiation pressure–to–gravity ratio β: $v = [(1-\beta)GM/r]^{1/2}$ at the distance r from the star, where β depends on the grain size. As a consequence, there are two subregions, corresponding to different behavior of the vaporization rate with distance. Consider a collision between a pair of grains in bound orbits, with the radiation-to-gravity ratios β_1 and β_2. In the first subregion, very near the star, the relative velocity (averaged over orbital inclinations) is above the vaporization threshold for any combination of β_1 and β_2; that is, for all sizes of orbiting grains. The outer limit of this subregion can be seen as the break in the initially power-like increase of the vaporization rate with distance. With increasing distance from the star, the orbital velocities decrease so that the collision velocity can exceed the vaporization threshold only for the grains with large enough difference between β_1 and β_2. This is the second subregion, extending to the distance at which the average relative velocities between all orbiting grains fall below the vaporization threshold and the vaporization rate from this source falls sharply to zero. Note the difference between the limits of these subregions for different grain materials.

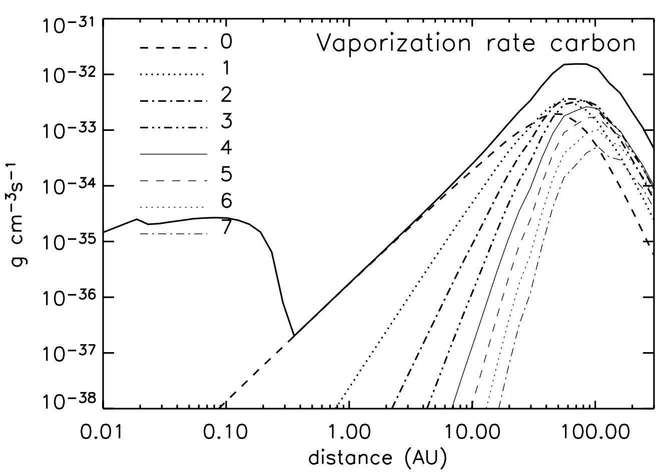

FIG. 9.—Same as Fig. 8, but for the case of the disk composed of carbon grains. The first eight generations of the β-meteoroids are included.

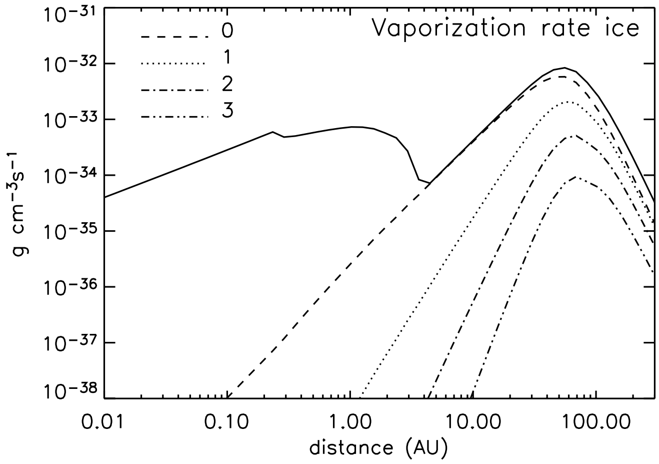

FIG. 10.—Same as Fig. 8, but for the disk composed of the grains with the properties of ice.

Beyond this distance, the only contribution to collisional vaporization comes from collisions involving β-meteoroids, which is dominated by collisions between β-meteoroids and orbiting grains. Although for the icy target vaporization is much more efficient than for any other case (see Fig. 2), the vaporization rate for carbon is strongly enhanced by the high velocities of the carbon β-meteoroids, leading to a cascade of higher generation β-meteoroids. Note that the cascade develops despite the fact that the disk is optically thin: the reason is the large multiplication factor (large $C_{\rm frag}$; Fig. 3). While for the cases of silicate and ice (Figs. 8 and 10) it is enough to include the first four generations of the β-meteoroids, the contribution from high generations of the carbon β-meteoroids to the vaporization rate remains significant at large distances (Fig. 9). Note that the contributions from higher generations become increasingly important at larger distances.

Our results correspond to the total mass production rate in the disk of 2.0×10^{13} g s^{-1} (collision model for ice), 5.5×10^{11} g s^{-1} (collision model for silicate), and 1.1×10^{14} g s^{-1} (collision model for carbon). The result for ice is of the same order of magnitude as the value of $10^{-13}\ M_\odot$ yr^{-1} estimated by Fernández et al. (2006) and higher by a factor of 3000 than the value of $10^{-16}\ M_\odot$ yr^{-1} of Lagrange et al. (1998) obtained, but in a completely different model. Contribution from the collisions between the grains of size above the blowout limit, which is restricted to a small region near the star, is very small (2.3×10^7 g s^{-1} for ice, 6.3×10^2 g s^{-1} for silicate, and 3.9×10^2 g s^{-1} for carbon).

It is instructive to compare the numerical results with an order-of-magnitude estimation of the vaporization rate based on the information presented in Figures 1–7. Consider the case of silicate grains at 100 AU. Since the number density of bound grains in the inner part of the disk is low, most of the β-meteoroids present at 100 AU originate from the part of the disk beyond a few times 10 AU from the star and so cannot reach high asymptotic velocities. A large velocity threshold ($v_{\rm th} = 19$ km s^{-1}) for vaporization means that only the β-meteoroids with the size corresponding to the value of β near the maximum, $a \sim 0.1\ \mu$m (Fig. 1), or, equivalently, to the maximum of v_∞, $m \sim 10^{-14}$ g (Fig. 7), can cause vaporization. Consider the contribution from the grains in the size interval for which v_∞ is above 80% of the maximum value. From Figure 7 it corresponds to the mass range of about 1.4×10^{-15} to 2×10^{-13} g, or, equivalently, the radius range 0.05–2.7 μm. The grain density in the disk at 100 AU in this size range can be estimated from Figure 4: for the $n = 0$

grains it is $N_m \sim 10^{-23}$ g cm^{-3}. A fraction of these grains (say, fN_m) present at 100 AU will have the velocity above the vaporization threshold. Let $\langle v \rangle > v_{\rm th}$ denote the average velocity of these grains and $\langle C_{\rm vap} \rangle$ the corresponding average of $C_{\rm vap}(v)$ (Fig. 2). The contribution to the vaporization rate at 100 AU is then approximately given by $N_m \langle v \rangle \langle C_{\rm vap} \rangle \Gamma$, where Γ is the geometrical cross section of the bound grains at 100 AU (the integral of the cross section πa^2 over the size distribution of the bound grains). The value of Γ at the distance r is determined by the optical thickness $\tau(r)$ of the dust disk by the relation $\Gamma 4r \sin \epsilon = \tau(r)$, where $\epsilon = 7°$ is the half angular thickness of the disk and $\tau(r)$ is given by equation (2) (we assume scattering efficiency of 2): at 100 AU, $\Gamma \sim 10^{-17}$ cm^{-1}. Taking $\langle v \rangle = v_{\rm th}$ and $\langle C_{\rm vap} \rangle = 3.5$ (Fig. 2), we obtain the vaporization rate of $\sim 6.6f \times 10^{-34}$ g cm^{-3} to be compared to $\sim 0.5 \times 10^{-34}$ g cm^{-3} of Figure 8, implying that $f \sim 0.1$. Observe that only the β-meteoroids originating within some region $r < r_m$ ($r_m < 100$ AU) from the star will be at 100 AU accelerated to the required high (larger than $v_{\rm th}$) velocity. The value of r_m can be found from equation (4) by solving the condition $v_r(r = 100\ \text{AU},\ r_m) > v_{\rm th}$ for the values of β corresponding to the selected interval of grain sizes: the result is $r_m \approx 31$ AU.

High vaporization rate for ice follows from low vaporization threshold (so that not only the grains with β close to maximum can cause vaporization) and large $C_{\rm vap}$ (Fig. 2). For carbon grains, despite high threshold for vaporization, the acceleration of the β-meteoroids is enhanced by high β (Fig. 1). In addition, high fragmentation rate leads to the density of β-meteoroids higher than for the other cases.

4. COMPARISON WITH THE OBSERVED GAS DENSITY: ESCAPE TIMES AND THE DISTRIBUTION IN THE ABSENCE OF BRAKING

The gas creation rate in the disk is not sufficient to determine the gas density distribution: for this, the escape rate of the gas atoms from the disk must also be known. If the outflow of the high-β species from the disk due to radiation pressure were not braked, one could derive the density distributions for these cases by assuming that this outflow is the dominant escape mechanism. This scenario is, however, unlikely in view of the recent observation by Fernández et al. (2006) that different species in the gas disk are coupled together by Coulomb interactions. The unbraked outflow may occur in the parts of the disk characterized by low electron density and high enough radiation pressure: this may happen in the region away from the disk midplane.

If the collisional dust vaporization rate is the dominant gas production mechanism in the disk, the escape times of the gas species can be estimated from the observed column densities. We use the equation $Q - n/t_{\rm esc} = 0$, where Q is the production rate and n is the density of the gas species. Let $\sim 7 \times 10^{-33}$ and $\sim 10^{-34}$ g cm^{-3} s^{-1} be the average gas production rates for the cases of ice and silicate, respectively, over the distances of the order of 100 AU (Figs. 10 and 8). The column densities $n_{\rm col}$ of different species we take from Roberge et al. (2006). Assuming that the average gas density in the disk is given by $n \sim n_{\rm col}/100$ AU and using the relative abundances for the chondrites or the Halley comet dust, we then obtain, for the case of high-β species (Si, Fe, Ca, Mn), the escape times of the order of 10^{10} s (ice) or 10^{12} s (silicate). The lifetime of a gas atom in the disk estimated by Fernández et al. (2006) is of similar order (10^4–10^5 yr).

In the absence of braking, the high-β ions soon after the release will move radially, forming a gas disk, with the initial velocity at release leading to some increase in the disk opening angle relative to the dust disk. If the braking is present, the radial outflow is suppressed and the escape from the disk in the direction perpendicular to the disk plane becomes more likely. The high-β ions that leave the disk and become free from the action of the braking force would then become accelerated and escape away from the system. For the high-β species the escape time can be then estimated as the time needed to reach the nearest boundary of the disk. In the case of the low-β species leaving the disk is not equivalent to the final escape, since the ions stay in bound orbits and may reenter the disk.

Taking ~ 10 AU as the average distance L to the disk boundary and $v \sim 2$ km s^{-1} as the average ion velocity perpendicular to the disk, the escape time for the high-β ions is then $L/v \sim 10^9$ s assuming that the ions move freely. If the mean free path λ for the ions is much less than L, we can assume that the motion is diffusive, with the diffusion coefficient $D = \frac{1}{3} v\lambda$. The escape time is then L^2/D. The escape times $\sim 10^{10}$ and 10^{12} s needed to maintain the observed column densities correspond to $\lambda \sim 10^{13}$ and 10^{11} cm, respectively. Note that the Larmor radius of a Ca II ion moving at 2 km s^{-1} in a magnetic field B is of the order $\sim 10^9(\mu{\rm G}/B)$ cm, so that a magnetic field of 0.01 μG would be sufficient.

We conclude that, if the braking in the disk is present, the dust vaporization rate obtained in our model may be able to explain the observed column densities. For a definite conclusion a detailed consideration of the escape processes is necessary.

In the absence of braking it is straightforward to calculate the density distribution of the high-β gas species assuming that the dominant escape mechanism is the streaming of the atoms away from the star caused by the radiation pressure. The result may be regarded as a lower limit on the high-β gas density from dust vaporization. It can also be relevant for the case of the high-β species produced in the disk but escaping away from the disk plane: the radiative acceleration, prevented from operating in the dense part of the disk, would then become important.

We assume that the source of gas described by the production rate $Q(r)$ (cm^{-3} s^{-1}) has a spherically symmetric distribution in space within some range of the latitude angle from the disk midplane. Let the source bodies be moving in circular orbits at Keplerian speed. Consider first the case when the initial speed of gas particles relative to the source is much less than the orbital velocity. If there are no losses (like ionization), the number density $n(r)$ of gas particles at the distance r from the star can then be expressed as

$$n(r) = \int_{r_{\rm min}}^{r} dr_0 \left(\frac{r_0}{r}\right)^2 \frac{Q(r_0)}{v_r(r,\ r_0)}, \tag{3}$$

where $v_r(r,\ r_0)$ is the radial velocity at r of the atom released at r_0:

$$v_r(r,\ r_0) = \left[\frac{GM}{r}\left(\frac{1}{x} - 1\right)(2\beta + x - 1)\right]^{1/2}. \tag{4}$$

Here G is the constant of gravitation, M is the star mass, and $x = r_0/r$. The value of the radiation pressure–to–gravity ratio β corresponds to the atom (ion) considered. The azimuthal velocity of the atom at r is

$$v_\phi(r,\ r_0) = \left(\frac{GM}{r} x\right)^{1/2}. \tag{5}$$

It should be noted that in the case of the atoms released due to vaporization, the initial velocity will be of the order of a few kilometers per second, which is comparable to the orbital speeds in the β Pictoris dust disk. However, for large-β species, the above equations provide a reasonable approximation. To see this, consider the case of nonzero initial velocity v_{r0} in radial direction. The expression for $v_r(r, r_0)$ becomes

$$v_r(r, r_0) = \left[v_{r0}^2 + (GM/r)(1/x - 1)(2\beta - 1 + x)\right]^{1/2}, \quad (6)$$

which at $\beta \gg 1$ can be written as

$$v_r(r, r_0) = (2\beta GM/r)^{1/2}\left[1/x - \left(1 - a^2\right)\right]^{1/2}, \quad (7)$$

where $a^2 = v_{r0}^2/(2\beta GM/r) \ll 1$ if β is large. That is, the effect of v_{r0} vanishes in the large-β limit. A similar argument works for the case of initial velocity in nonradial direction: if the radiation pressure effect is strong (high β), the released atoms would soon start moving in approximately radial direction, and the escape to high latitudes (transverse to the disk) could be neglected.

A high ionization rate in the β Pictoris disk implies that the atoms released as neutrals will soon become ionized. The dynamics of the ions may be significantly different from the neutral atoms because of the stellar magnetic field. Also, the value of β changes on ionization. In this discussion we neglect the effect of the magnetic field.

Consider the case of Ca II ions, expected to be the dominant state of Ca in the disk. Assuming that Ca I converts to Ca II immediately after release, we can use equation (3) to estimate the Ca II density distribution and the column density in the disk. We assume $\beta = 50$ for Ca II. The abundance of Ca in the grain material we take to be 1.4×10^{-2} by mass. The calculated density distribution is shown in Figure 11, assuming that $\beta = 50$ for the Ca II ion (Fernández et al. 2006). The corresponding column densities along a radial direction are 2.1×10^{10}, 7.3×10^{11}, and 3.1×10^{12} cm^{-2} for the grains with the collisional properties of the astronomical silicate, ice, and carbon, respectively, to be compared with the values derived from observations: 1.2×10^{13} cm^{-2} (Lagrange et al. 1998) and 2.6×10^{13} cm^{-2} (Roberge et al. 2006).

To interpret this result, we should bear in mind the uncertainties of the collision model. Note that we have considered only the cases for which all grains in the disk are of the same composition: adding some high-β grains would increase the vaporization rate. The vaporized mass will be probably higher for the case of porous materials (see discussion below). Also, the dust collision rate may be higher when inhomogeneities in the dust distribution are taken into account.

We can also model the effect of some amount of braking by reducing the value of β. For the high-β species the density scales approximately as $1/\beta^{1/2}$. Assuming that the braking reduces β from 50 to about 1 would then correspond to the Ca II density increase by a factor of $\sim$7.

5. GAS FROM DUST: OTHER MECHANISMS

Collisional vaporization is not the only gas production mechanism involving dust grains. We now briefly discuss two other processes: the stellar wind–dust interaction and sputtering from the dust surface. We do not consider sublimation since it would be limited to the inner region of the disk. At larger distance from the star sputtering is more important than sublimation (Mukai & Schwehm 1981).

The stellar wind–dust interaction leading to the release of neutral atoms from the dust grain surface was invoked in an attempt to explain the observations by the *Ulysses* spacecraft of the pickup ions originating near the Sun (Mann & Czechowski 2005). Two possible processes were considered. The atoms of solar wind origin can be implanted below the surface of the grains and released (in the neutral state) on impact of a solar wind ion. In the other process, applicable to small dust grains, a solar wind ion passing through the grain emerges slowed down and neutralized.

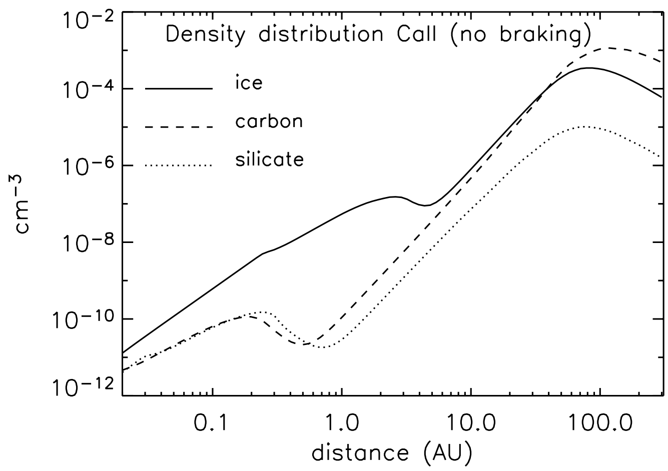

FIG. 11.—Calculated number density distributions of Ca II in the disk assuming a dust vaporization source and no braking. The models illustrated are the same as in Figs. 8, 9, and 10. Only the first four generations (eight for the carbon case) of the β-meteoroids are included. See the text for detailed discussion.

The rate of release of neutral atoms from the dust as a result of this process is given by the product of the "dust geometrical cross section" Γ [a size-integrated product of the dust number density and the frontal area of the grain: $\Gamma \equiv \int da\,(dn/da)\pi a^2$] and the stellar wind flux intensity. The value of Γ in the β Pictoris case is of the order 10^{-17} cm^{-1} at $r \sim 60$ AU from the star.

If one assumes that the β Pictoris wind is stronger by a factor of 10^4 compared to the solar wind (this possibility is not excluded by observations; Bouret & Deleuil 2003), the stellar wind flux at 60 AU would be of the order 10^9 particles (cm^2 s)$^{-1}$, leading to the gas production rate of 10^{-8} atoms (cm^3 s)$^{-1}$. Since the atoms from this source would be predominantly hydrogen, the mass production rate at 60 AU would be of the order of 10^{-32} g (cm^3 s)$^{-1}$, which is comparable to the collisional vaporization rate obtained in our model for the carbon and ice cases, but with different (stellar) abundances.

The stellar wind flux rises as $1/r^2$ toward the star. The behavior of the gas production rate due to stellar wind impact depends on how the dust density behaves in this limit. If the disk optical thickness behaves according to equation (2), the dust geometrical cross section at $r \ll r_m$ is proportional to r and the gas production rises toward the star. Near 5 AU the dust geometrical cross section is of the order of 2×10^{-18} cm^{-1} and the gas production rate is $\sim3\times10^{-31}$ g (cm^3 s)$^{-1}$. The rise in the gas production rate would be, however, restricted to small volume. The total gas production rate from the region within 60 AU from the star due to the stellar wind impact mechanism is then $\sim10^{13}$ g s^{-1}, leading to the average rate per unit volume of 10^{-32} g (cm^3 s)$^{-1}$. This probably provides an upper estimate since the number density in the inner disk is depleted (note that the dust density profile used in Fernández et al. [2006] falls faster toward the star than in our model). Estimates for the inner depletion zone inward from 20 AU vary for different studies (Mann et al. 2006) due to a lack of direct observations.

The other mechanism is sputtering. If initiated by the stellar wind protons of energy $\sim$1 keV, the sputtering yield would be of the order 10^{-2} (Tielens et al. 1994) and higher ($\sim$0.7) if the grain material were ice. The sputtering rate would then be, in terms of number of atoms, about 0.01 of the rate for the solar wind impact mechanism discussed above. Since the sputtered atoms would be coming from the grain material, the gas production rate in terms of mass would be not much less than for the solar wind impact mechanism; that is, of the order of a few times 10^{-33} g (cm^3 s)$^{-1}$. However, if the yield value for ice can be used, the gas production rate from sputtering by the stellar wind may be as high as 10^{-31} g (cm^3 s)$^{-1}$, which is significantly higher than the rate for collisional vaporization following from our calculations.

Our discussion of the stellar wind–related processes in this section was restricted to the case of the simplest stellar wind–dust grain interaction. The possible effects of the stellar wind on the dust disk and the gas dynamics in the β Pictoris case require a detailed study.

If the amount of gas in the disk is large, there is also a possibility of sputtering by gas particles colliding with the grains. For appreciable sputtering yields the gas temperature would, however, have to be very high (10^2 eV; Tielens et al. 1994).

6. VELOCITY DISTRIBUTIONS ALONG THE LINE OF SIGHT IN THE ABSENCE OF BRAKING

In this section we consider the differential distributions in velocity relevant for remote observation of the particles in circumstellar disks that are released from orbiting bodies and accelerated away from the star by radiation pressure. We find that, even in the absence of braking, the emission or scattering spectra from these particles can include a peak at the frequency corresponding to the Doppler shift by the velocity equal to the Keplerian velocity for the orbit of radius equal to the distance by which the line of sight bypasses the star. That is, the presence of a peak at Keplerian velocity is not by itself a proof that the emitting gas corotates.

Although the motivation for this study was provided by the observations of the emission from the β Pictoris gas disk, we do not claim that the above result is relevant for this case. In fact, our result does not explain the lack of outflow signatures in the absorption spectrum or the lack of a broad component in the emission spectrum, which are the main observational arguments for braking for the case of β Pictoris. Also, a natural braking mechanism was identified recently by Fernández et al. (2006). Nevertheless, it seems to us that this result may be of more general interest, particularly in view of an increasing number of observations of the dust disks. In the case of β Pictoris, a possible application may be to the gas in the low-density region away from the disk plane, where the braking could be less efficient. Note that our result is not restricted to emission from gas particles: a similar phenomenon would be expected for scattering off the high-β dust grains.

Consider the case of remote observation of the particle distribution along a line of sight positioned in the midplane of the circumstellar disk. Let d be the closest distance from the line of sight to the star and w be the distance from the point nearest to the star along the line of sight, with $w > 0$ corresponding to the direction toward the observer (Fig. 12). The radiation from the moving particles will be observed shifted in frequency due to Doppler effect. The shift is determined by the component of the particle velocity along the line of sight $v_{\rm LOS}$. In the spherical coordinates with the z-axis perpendicular to the disk,

$$v_{\rm LOS} = \frac{w}{r} v_r(r, r_0) + \frac{d}{r} v_\phi(r, r_0), \quad (8)$$

where w is the length parameter along the line of sight (Fig. 12). We restrict attention to the case of particles moving in the orbits with low inclination relative to the disk and so assume that v_ϕ is approximately equal to the nonradial component of the particle velocity ("thin-disk approximation").

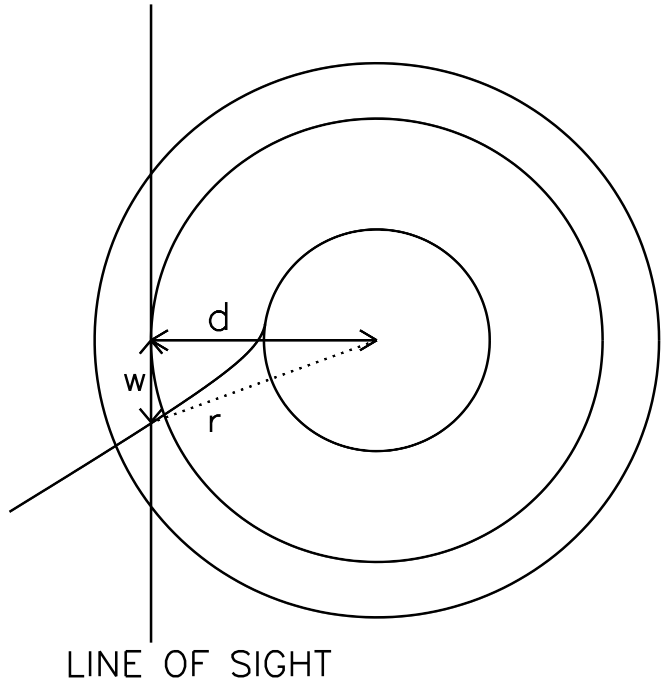

FIG. 12.—Schematic view of the disk plane. A trajectory of an atom released from a circular orbit is shown. The line of sight passes the star at the distance d; w is the coordinate along the line of sight counted in the direction toward the observer from the point of closest approach to the star.

The distribution of particles along the line of sight with respect to $v_{\rm LOS}$ is characterized by the column density $dN/dv_{\rm LOS}$:

$$\frac{dN}{dv_{\rm LOS}} = \int dw \int dr_0 \int d\boldsymbol{v}_0 \left(\frac{r_0}{r}\right)^2 \frac{Q(r_0, \boldsymbol{v}_0)}{v_r(r, r_0, \boldsymbol{v}_0)} \times \delta\left[\frac{w}{r} v_r(r, r_0, \boldsymbol{v}_0) + \frac{d}{r} v_\phi(r, r_0, \boldsymbol{v}_0) - v_{\rm LOS}\right], \quad (9)$$

where $Q(r_0, \boldsymbol{v}_0)$ is the differential rate (per unit volume and unit velocity) of gas particles being released from the parent bodies moving in circular Keplerian orbits of radius r_0 at the initial velocity $\boldsymbol{v}_0$ relative to the parent body, and $v_r(r, r_0, \boldsymbol{v}_0)$ and $v_\phi(r, r_0, \boldsymbol{v}_0)$ are the radial and azimuthal components of the particle velocity at the distance r. The intensity of radiation will be proportional to the similar integral with an extra factor of $1/r^2$ in the integrand.

If the particles are released at zero velocity relative to the parent body,

$$\frac{dN}{dv_{\rm LOS}} = \int_{-\infty}^{\infty} dw \int_{r_{\rm min}}^{r} dr_0 \left(\frac{r_0}{r}\right)^2 \frac{Q(r_0)}{v_r(r, r_0)} \times \delta\left[\frac{w}{r} v_r(r, r_0) + \frac{d}{r} v_\phi(r, r_0) - v_{\rm LOS}\right], \quad (10)$$

where $Q(r_0)$, $v(r, r_0)$, and $v_\phi(r, r_0)$ are the same as in equations (3)–(5). Note that $r \geq r_0$ since the radial velocity is positive in this case. Using the Dirac delta function, the integral over r_0 can be performed:

$$\frac{dN}{dv_{\rm LOS}} = \int_{-\infty}^{\infty} dw \sum_i \left[\left(\frac{r_0}{r}\right)^2 \frac{Q(r_0)}{v_r(r, r_0)} \frac{1}{|dv_{\rm LOS}/dr_0|}\right]_i \times \Theta(r - r_{0i})\Theta(r_{0i} - r_{\rm min}), \quad (11)$$

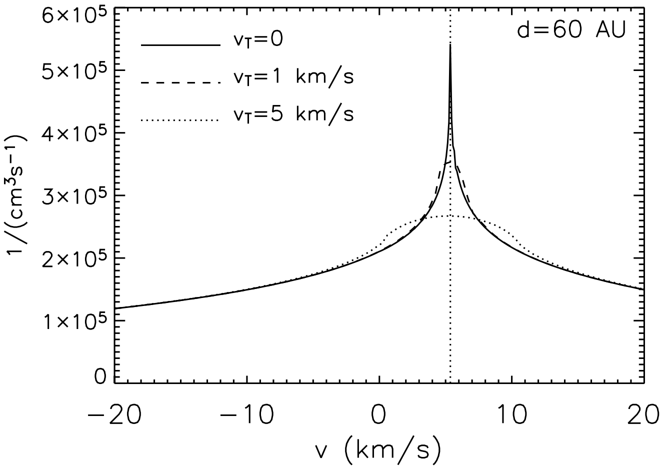

FIG. 13.—Calculated differential column densities $dN/dv_{\rm LOS}$ along a line of sight passing at 60 AU from the star for different initial velocity spread. The azimuthal velocity on release was assumed to be uniformly distributed within $(-v_T, v_T)$ from the orbital velocity of the parent body. The solid line corresponds to zero release velocity. The vertical dotted line indicates the orbital velocity at 60 AU.

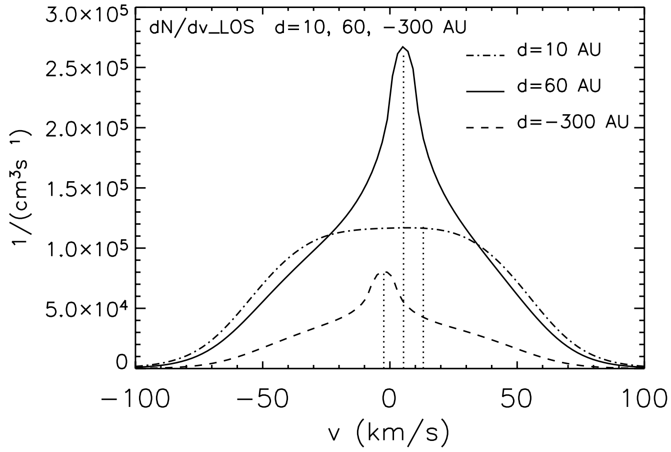

FIG. 14.—Calculated $dN/dv_{\rm LOS}$ for the lines of sight passing through different regions of the disk, at the distances 10, 60, and 300 AU from the star. For the 300 AU case, the line of sight passes on the side of the star where the orbital motion is directed away from the observer; we use the convention that $d < 0$ for such a case. In the case $d = 10$ AU the peak is not visible, since the gas creation rate increases along the line of sight away from the $w = 0$ point. Initial velocity spread $v_T = 5$ km s^{-1} was assumed. Vertical dotted lines show the Keplerian velocities at $d = 10$, 60, and -300 AU.

where the expression in square brackets is evaluated at the points $r_{0i} = r_{0i}(w, v_{\rm LOS})$ for which the argument of the delta function vanishes. A detailed analysis shows that the number of solutions r_{0i} depends on the values of w, β, and $v_{\rm LOS}$ and the maximum number of solutions is 3.

An interesting effect is that there is a singularity in the w integral in equation (10) leading to a peak in the distribution $dN/dv_{\rm LOS}$ at the velocity $v_{\rm LOS} = v_{\rm orb}(d)$, the Keplerian velocity for the orbit at the distance d from the star. This singularity (which is logarithmic) becomes regularized if the initial velocity spread or the spread of orbital inclinations is taken into account, but it may leave a finite maximum in the velocity distribution. The prominence of the peak depends, in particular, on the distribution of the gas source $Q(r_0)$ in the disk. One consequence is that the observation of the peak in gas emission from the disk corresponding to the orbital velocity is not inconsistent with radial acceleration of the gas and does not require "braking". Emission from the high-velocity particles is present in the spectrum but has a lower intensity.

In Appendices B and C we give an analytical argument for the presence of the singularity. Results from numerical calculations, both for the singular (zero release speed) and for the finite peak cases, are shown in Figures 13 and 14. In addition, we note that for the case of uniform gas production in the disk the peak is suppressed in the velocity distribution, although in the emission spectrum (with an additional $1/r_0^2$ factor due to stellar radiation) it is still visible. For the case of the gas originating from the dust, the source distribution would be likely to fall at large distances at least as steep or steeper than the dust density (which behaves as $1/r_0^3$ if eq. [2] is used).

The interpretation of the peak in the Doppler-shifted radiation is as follows. The peak is due to particles released in the immediate vicinity of the line of sight, near the point where the distance from the star to the line of sight is minimal: $r_0 = d$. Since the particles' radial speed at the time of release is small, their number density is large at this point and the contribution from the region $(r_0,\ r_0 + dr_0)$ with $r_0 \approx d$ to the density at the line of sight would be also large. If one would be interested in deriving the distribution in radial velocity, the high value of the number density would be compensated for by the high value of radial acceleration: dv_r/dr_0 since $dn/dv_r = (dn/dr_0)/(dv_r/dr_0)$. However, for the distribution $dn/dv_{\rm LOS}$ calculated near $w = 0$ the radial velocity has a zero component along the line of sight and this compensation does not occur. As a result, the particles released near $w = 0$ and $r_0 = d$ give a large contribution to $dn/dv_{\rm LOS}$ with the effect that there is a peak reflecting their initial velocity at the moment of release. This peak may be masked if there is a large contribution to low $v_{\rm LOS}$ from other parts of the line of sight (see Fig. 14).

In all figures in this section we use the same model of the gas production rate, close to our model of collisional vaporization for the case of ice. The distributions are calculated for a gas species with the abundance in the grain material 1.4×10^{-2} by mass (the value assumed for Ca). The value of β if not indicated otherwise is taken to be 100. The sign of d is positive if the line of sight passes the star on the side at which the orbital motion is directed toward the observer (leading to the blueshift in the spectrum), and negative for the opposite case.

Figure 13 shows $dN/dv_{\rm LOS}$ calculated for the line of sight at the distance $d = 60$ from the star. The case of the gas particles released at zero velocity relative to the parent body corresponds to the solid line. To illustrate the effect of the initial velocity spread on the peak in $dN/dv_{\rm LOS}$, two cases with nonzero initial velocity are also shown. The particles were assumed to have initial azimuthal velocity at release distributed uniformly between $-v_T$ and v_T relative to the Keplerian velocity.

The distributions for the line of sight passing through different parts of the disk are shown in Figure 14. Observe that for the line of sight corresponding to small d the peak at $v_{\rm orb}(d)$ is absent because the parts of the line of sight away from $w = 0$ pass through the region of the disk with a higher gas creation rate.

In the above discussion, we have assumed that the particles move solely under the influence of the radiation and gravity forces with fixed value of β and that no losses occur. In particular, the possibility of ionization to the state with low β was neglected. Since the neutral species with high β are all easily ionized except for the case of cool stars (Fernández et al. 2006), the results are more likely to be relevant for the ionized species with high β in the dominant ionization state (like Ca II) provided that the effects of magnetic field and stellar wind on the particle motion can be neglected.

The presence of the peak at Keplerian velocity in the velocity distribution along a line of sight does not require braking.

Therefore, observation of the peak does not provide evidence that braking of the outflowing gas occurs. However, the accelerated atoms contribute to the wings of the velocity distribution and of the spectrum. For the case of the line of sight passing through or very close to the star, the peak at Keplerian velocity is absent or suppressed (see Fig. 14, the $d = 10$ case) and the accelerated particles would be clearly seen.

7. DISCUSSION

We have estimated the contribution of dust vaporization to production of nonvolatile gas species in the β Pictoris disk. The distribution of the dust grains with the size above the blowout limit (about 2 μm) was assumed to fit the disk optical thickness data. Collisional fragmentation of these grains leads to production of smaller fragments, which are accelerated by the radiation pressure. Vaporization of the dust material occurs as a result of collisions with these small projectile grains. We found that the mass production rate from this source depends strongly on the optical and mechanical parameters of the dust grains composing the disk. Small high-β grains, with the optical properties similar to carbon, are most efficiently accelerated by radiation pressure and so could be the main agents causing vaporization. The largest vaporized mass is obtained for the case of icy target grains. If uniform composition is assumed for all grains in the disk, the total mass production rate is 2.0×10^{13} g s^{-1} (ice), 5.5×10^{11} g s^{-1} (silicate), and 1.1×10^{14} g s^{-1} (carbon). The gas source distribution has a maximum near the distance from the star corresponding to the maximum density of dust (60 AU in our model) and decreases both outward and inward from this distance.

The density of the produced gas species is not determined by the production rate alone, but it is necessary to know also the escape and the loss rates. In the case of the disk of β Pictoris, this is complicated by the need for a braking mechanism to keep the high-β species from reaching high radial velocities. We have estimated the escape times needed in our model to produce the column densities of the high-β gas species as derived from observations. These are $\sim10^{10}$ and 10^{12} s for the case of ice and silicate grains, respectively. These values are close to the lifetimes estimated by Fernández et al. (2006). Also, they do not require unreasonably short mean free paths of the ions in the disk.

We did not try to construct a detailed model of the gas disk that would include the braking and escape processes and could give predictions for the gas density profiles that could be compared with observations. We have, however, calculated the density distributions and column densities of the high-β Ca II ions under the assumption that there is no braking: the results can be regarded as lower limits on actual densities and in fact are below the values estimated from the spectroscopic data. The density profiles are qualitatively different from those deduced from observations: in particular, they decrease toward the star inward from $\sim$60 AU, and the decrease at large distance is much slower. Note that the low-density value and the slow falloff at large distances can be qualitatively understood as due to neglect of braking. Moreover, a decrease of the observed column density with increasing distance from the star may be partly due to the effect of the magnetic field deflecting ions to higher latitudes.

We also calculated the velocity distributions (integrated along a line of sight bypassing the star) of the high-β gas particles released from the dust grains assuming that there is no braking. Although soon after release the particles are accelerated to high radial velocity, in their velocity distribution along a line of sight passing through the disk at some distance from the star there appears a peak at the velocity of Keplerian orbital motion for the circular orbit tangent to the line of sight. This would lead to a peak in the emission spectrum at the Keplerian velocity. The emission from accelerated particles would appear in the wings of the spectrum. The presence of the peak at Keplerian velocity is therefore not by itself an argument for braking. However, this peak does not occur for the lines of sight passing very near the star, and in the absence of braking the high-velocity particles would clearly contribute to the absorption features. In the case of β Pictoris the presence of a braking mechanism is suggested since there is no signature of radial acceleration in the absorption spectra. In addition, a natural braking mechanism was recently proposed (Fernández et al. 2006).

Some parameters that enter our calculations are either not directly measured or largely based on model assumptions. These are (1) the dust spatial number density and the size distribution, (2) the model of collisional vaporization, and (3) the dust composition and β-values.

Dust distribution.—The dust distribution used in our calculations, while based on observations, is simplified. In particular, we assume a standard size distribution and a smooth spatial distribution of dust. However, spatial structures are observed in the disk. Recent discussions suggest that the spatial variations are caused by the spatial distribution of the planetesimals that serve as parent bodies of the dust (Mann et al. 2006). Such local variations are also considered for the study of collision avalanches that were recently studied in detail (Grigorieva et al. 2007). Within the range of distances corresponding to gas observations, the spatial features in the dust density distribution were found between 14 and 82 AU from the star in the thermal emission brightness indicating the presence of rings (Wahhaj et al. 2003). As we have pointed out for the case of the circumsolar dust cloud (Mann & Czechowski 2005), the local enhancements in the dust density would increase the total collision rate between the grains. Consequently, in the β Pictoris dust disk the flux of β-meteoroids should increase outward from local dust density enhancements. Note also that the polarization measurements inward from 30 AU point to the presence of micrometer-sized grains possibly produced as collision fragments (Okamoto et al. 2004).

Model of collisional vaporization.—Our calculations of the amount of vapor production are based on semiempirical formulae. The material parameters used agree with laboratory measurements in the limit of small relative velocities, solid extended targets, and large sizes of targets and projectiles (Tielens et al. 1994).

The energy deposit of the impact causes ionization of target and projectile material that subsequently recombines in the expanding plasma cloud. Due to the relatively low temperature in the plasma cloud, recombination of the produced ions leads to primarily neutral and singly charged compounds. Hornung & Kissel (1994) give a temperature of 10^4 K for the vapor, while from measurements of a 5.3 km s^{-1} impact, Sugita et al. (1997) derive a temperature of 6000 ± 800 K for an impact angle of 60° from horizontal direction and a value of 4200 ± 700 K for an impact angle of 30° from horizontal direction. These temperatures correspond to thermal velocities of the order of kilometers per second, which are within the range of release velocities discussed in §§ 4 and 7.

We also think that our assumption of initially neutral species can be justified: for the case of SiO_2 particles, Hornung et al. (2000) concluded from numerical simulations of the impact process that for collision velocities below 40 km s^{-1} there is no significant amount of ionized species contained in the vapor. They point out, however, that certain charge and vapor production is observed in experiments at lower velocities already. For higher velocities the fraction of ions depends critically on the ionization potential of the species: while for an 80 km s^{-1} impact about half of the Si is ionized, the fraction of ionized O is still below 1%. In any case, significant fractions of doubly ionized species occur only at speeds beyond 100 km s^{-1} and are not important for our considerations here. It should be noted that also the formation of molecular species is possible, although it is hard to quantify.

For the case of small particles and high impact velocities, the expansion time might be shorter than time spans for recombination, so that different conditions apply; further surface processes and vaporization of ejecta particles may play a role (see, e.g., Hornung & Kissel 1994). Laboratory experiments on macroscopic scales have shown that the impact process varies with the porosities of materials (Nakamura et al. 1994), as well as for different meteorites (Tomeoka et al. 2003).

The dust composition and β-values.—Information about material composition in the β Pictoris system is scattered: features in the thermal emission observations indicate the presence of silicates. Guided by a model of interstellar dust being agglomerated to form the grains in the disk, Li & Greenberg (1998) explained the thermal emission brightness over a broad spectral range assuming a mixture of high porosity particles comprised of crystalline silicate and amorphous material with silicate chemical composition, organic refractories, and ice at distances larger than 100 AU from the star. Tamura et al. (2006) explain the measured polarization between 50 and 120 AU in the K-band scattered light brightness using a model of ice-filled fluffy aggregate particles.

Aside from the models of the collision process, dust material composition also influences optical properties and therefore the β-values. The β-values used in the calculations were obtained from model calculations for spherical homogeneous compact particles (Köhler & Mann 2002). While the value of β used here for carbon grains seems very high for large porous particles, it may be more realistic for the small grains that act as building blocks for larger particles.

Although our study was restricted to the case of β Pictoris, some conclusions can be reached also for the case of other circumstellar disks. Collisional vaporization requires that the collision velocity be higher than the vaporization threshold $v_{\rm th}$ defined by the composition of the dust grain. The β-meteoroids that can initiate vaporization must then originate within some maximum distance r_m from the star. This distance is determined by the maximum value β_m of the radiation-to-gravity ratio for the grains. Since a grain with the radiation-to-gravity ratio β released at the distance r from the star can be accelerated by radiation pressure to the maximum velocity $(2\beta - 1)^{1/2} v_{\rm orb}(r)$, it follows that $r_m = [v_{\rm orb}(1\ {\rm AU})/v_{\rm th}]^2(2\beta_m - 1)$ AU. Collisional vaporization by the β-meteoroids requires that there should be enough of the dust material in the $r < r_m$ part of the disk. Consequently, for the disks with large gaps the collisional vaporization is suppressed. As an example, consider the case of the debris disks of three hot stars: Vega ($T \sim 9553$ K), Fomalhaut ($T \sim 8760$ K), and HD 141569 ($T \sim 10{,}000$ K). The corresponding values of β_m, r_m, and the observed approximate inner cutoff radii $R_{\rm inner}$ of the debris disks (Su et al. 2005; Kalas et al. 2005; Marsh et al. 2002) are listed in Table 1. The necessary condition for collisional vaporization, $r_m > R_{\rm inner}$, is satisfied for the cases of Vega and HD 141569, while for Fomalhaut (which is cooler than the other two) $r_m \sim R_{\rm inner}$. The values of β_m were calculated by Köhler & Mann (2002) using Mie approximation for uniform spherical grains and the blackbody spectra.

For cool stars like AU Microscopii ($T \sim 3600$ K) the radiation pressure is too weak (Augereau & Beust 2006) to produce β-meteoroids: even in the flare state ($\beta \sim 0.5$) it would not be able to accelerate the grains to the velocity required for vaporization. However, the stellar wind for a young star like AU Mic may be significantly stronger than for the Sun, producing a significant plasma Poynting-Robertson drag on the grains (Minato et al. 2006; Plavchan et al. 2005; Augereau & Beust 2006) and, if the wind is at least $\sim 10^3$ times the solar wind, ejecting the grains with sizes less than ~ 0.2 μm (Plavchan et al. 2005). The possibility of collisional vaporization depends on the maximum velocity that could be reached by these grains. Since for the grains near the blowout limit the asymptotic velocity is small, and the smaller grains (< 0.05 μm for the case of the solar wind; Minato et al. 2006) are penetrated through by the stellar wind ions with only partial momentum transfer, it is not clear that the required velocity could be reached. Strong stellar wind will, however, produce some neutral gas by interacting with the bound grains, as discussed in § 5: contrary to dust vaporization, this gas will have stellar wind abundances. Detection of a gas component in the debris disks like AU Mic would therefore be an indicator for strong stellar wind.

TABLE 1

Values of β_m, r_m, and $R_{\rm inner}$ for Selected Hot Stars

Hot Star	β_m	r_m (AU)	$R_{\rm inner}$ (AU)
Vega	23	280	86
Fomalhaut	11.4	125	133
HD 141569	80	912	100

8. CONCLUSIONS

Our results indicate that collisional vaporization of dust may be an important source of gas in the disk of β Pictoris. The gas production rates calculated in our model are high enough to account for the observed column densities provided that the escape times of the gas from the disk are of the order 10^{10}–10^{12} s, which is not unreasonably high. For high-β species this requires that some braking mechanism be present. If braking were absent, we found that for the assumed model parameters the collisional vaporization of dust would produce the amount of high-β species that are below (by a factor between ~ 1000 and ~ 10) the number densities derived from observations. The total mass vaporization rate calculated in our model is of the same order of magnitude as other authors' estimations of the required gas production rate. The value for ice is close to the value of 10^{-13} $M_\odot$ yr^{-1} estimated by Fernández et al. (2006). We note that the actual collision frequency of the dust and therefore the gas production rate may be higher than assumed in the model: observations indicate that the dust around β Pictoris is not smoothly distributed and the local variations in dust density may enhance the collisional vaporization.

The species produced by collisional vaporization are usually not in ground state, and observed line intensities are influenced by the initial temperature of the produced vapor that determines the population of the different energy levels of the species. The element abundances in the gas following from dust vaporization would be close to the dust composition. The dust may be comparable to the cometary dust in our solar system rather than to the meteoritic composition. Therefore, a higher abundance of C compared to the meteoritic abundance is plausible, but we cannot at present predict the amount of carbon enhancement compared to other elements.

From calculations of the gas velocity distributions we conclude that the observation of the gas emission peak at the Keplerian velocity does not necessarily require braking of the outflowing gas component.

We think that future studies of the braking mechanism should take into account the possibility of higher temperatures of the gas, as well as the possibility of the presence of the stellar wind. More observational results on the circumstellar gas components are extremely desirable.

This research has been supported by the German Aerospace Center, DLR (project "Rosetta: MIDAS, MIRO, MUPUS" RD-RX-50 QP 0403), and by the 21st Century COE Program "The Origin and Evolution of Planetary Systems" of the Japanese Ministry of Education, Culture, Sports, and Technology (MEXT).

APPENDIX A

THE MODEL OF DUST COLLISIONS AND COLLISIONAL VAPORIZATION

Our model of individual dust collisions is based on that of Tielens et al. (1994). For a collision at a relative velocity $v_{\rm rel}$ between two grains (of the same composition) with masses m_1 (target) and m_2 (projectile), the fragmented ($m_{\rm frag}$) and vaporized ($m_{\rm vap}$) mass of the target is $m_{\rm frag} = C_{\rm frag} m_2$ and $m_{\rm vap} = C_{\rm vap} m_2$, with $C_{\rm vap}$ and $C_{\rm frag}$ dependent on the collision velocity (see Figs. 2 and 3). If $C_{\rm vap} m_2$ exceeds m_1 (the mass of the target), the whole target is vaporized: $m_{\rm vap} = m_1$. If $C_{\rm frag} m_2$ is larger than $m_1 - m_{\rm vap}$, then $m_{\rm frag} = m_1 - m_{\rm vap}$. The mass distribution of fragments is given by a single power law

$$\frac{dN}{d\log m} = Cm^{-\eta} \qquad (m < m_L), \tag{A1}$$

where $\eta = 0.76$. The constant C is determined by the requirement that the total mass in fragments is equal to $m_{\rm frag}$:

$$\int_0^{m_L} d\log m\, Cm^{-\eta} m = m_{\rm frag}. \tag{A2}$$

The largest fragment mass m_L depends on the masses, relative velocity, and the material parameters of the colliding grains:

$$\frac{m_L}{m_1} = \left(0.2\frac{v_{\rm cat}}{v_{\rm rel}}\right)^3, \tag{A3}$$

where $v_{\rm cat}$ is the critical fragmentation velocity. The values of $v_{\rm cat}$ for the case of the projectile with radius 5 nm and the target with radius 100 nm are 1.2×10^5 m s^{-1} (ice), 7.8×10^4 m s^{-1} (carbon), and 1.83×10^5 m s^{-1} (silicate). For other grain sizes they can be obtained using the formula

$$v_{\rm cat} = {\rm const}(m_1/m_2)^{9/16}. \tag{A4}$$

If the value of m_L obtained in this way exceeds 0.1 of the fragmented target mass, we set $m_L = 0.1 m_{\rm frag}$.

Let $\mu < m < M$ be the mass range of the grains and $f(m, r)$ denote the distribution $dN/dm\, d^3r$ of the grains in the bound orbits ($m > m_b$, where m_b is the blowout limit). The mass vaporization rate due to collisions between these grains is then given by

$$\int_{m_b}^{M} dm_1 f(m_1, r) \int_{m_b}^{M} dm_2 f(m_2, r) v_{\rm rel}(r, m_1, m_2)\sigma(m_1, m_2) m_{\rm vap}, \tag{A5}$$

where $\sigma(m_1, m_2) = \pi(a_1 + a_2)^2$ is the cross section for collision with a_1, a_2, the radii of the grains. We assume that the grains are compact and spherical with mass density ρ. Then

$$\sigma(m_1, m_2) = \frac{\pi\left(m_1^{1/3} + m_2^{1/3}\right)^2}{[(4/3)\pi\rho]^{2/3}}. \tag{A6}$$

The (number) production rate $Q_0(m, r)$ of $n = 0$ β-meteoroids of mass m per unit volume and unit mass interval due to collisions between the grains in bound orbits at distance r from the star is

$$Q_0(m, r) = \int_{m_b}^{M} dm_1 f(m_1, r) \int_{m_b}^{M} dm_2 f(m_2, r) v_{\rm rel}(r, m_1, m_2)\sigma(m_1, m_2) C m^{-\eta-1}\Theta(m_L - m), \tag{A7}$$

with $\mu < m < m_b$ and C and m_L determined as above. The production rate of the nth-order β-meteoroids is given by

$$Q_n(m, r) = \int_{m_b}^{M} dm_1 f(m_1, r) \int_{\mu}^{m_b} dm_2 \int_{r_{\rm min}}^{r} dr_0 \frac{r_0^2}{r^2}\frac{Q_{n-1}(m_2, r_0)}{v_r(r, r_0, m_2)} v_{{\rm rel},\beta}(r, r_0, m_1, m_2)\sigma(m_1, m_2) C m^{-\eta-1}\Theta(m_L - m). \tag{A8}$$

In this equation $v_r(r, r_0, m_2)$ is the radial velocity at r of the mass $= m_2$ β-meteoroid released at r_0 from the body in a circular Keplerian orbit [given by eq. (4) with $\beta = \beta(m_2)$], and $v_{{\rm rel},\beta}(r, r_0, m_1, m_2)$ is the average relative velocity at r between the mass $= m_2$ β-meteoroids released at r_0 and the mass $= m_1$ bound grains.

The average relative velocities between the projectile and the target grains used in the model are as follows: For the collisions between bound grains

$$v_{\rm rel}(r,\, m_1,\, m_2) = \frac{1}{(2\epsilon)^2}\int_{-\epsilon}^{\epsilon} d\theta_1 \int_{-\epsilon}^{\epsilon} d\theta_2 \left[v_1^2 + v_2^2 - 2v_1v_2\cos(\theta_1-\theta_2)\right]^{1/2}, \tag{A9}$$

where $\epsilon = 7°$ is the half-opening angle of the disk and v_1 and v_2 are the orbital speeds of the grains with the masses m_1 and m_2 with the radiation force taken into account: $v_i = \{[1-\beta(m_i)]GM/r\}^{1/2}$. For the β-meteoroid impact on the bound grains we use

$$v_{\rm rel,\beta}(r,\, r_0,\, m_1,\, m_2) = \left\{v_r(r,\, r_0,\, m_2)^2 + \left[v_\phi(r_0,\, r) - v_2\right]^2\right\}^{1/2}, \tag{A10}$$

where $v_\phi = (GMr_0/r^2)^{1/2}$ is the azimuthal speed at r of the β-meteoroid released at r and v_2 is the orbital speed of the target grain.

APPENDIX B

VELOCITY DISTRIBUTION ALONG THE LINE OF SIGHT

In the case of particles released from the parent bodies at zero relative speed, the distribution $dN/dv_{\rm LOS}$ has a logarithmic singularity at $v_{\rm LOS}$ equal to $v_{\rm orb}(d)$, which is the orbital speed at the distance d from the star. In this section we show how the singularity arises.

We denote

$$f(x,\, w) = \frac{w}{d}\tilde{v}_r(x) + \tilde{v}_\phi(x). \tag{B1}$$

The delta function under the x integral (obtained from the r_0 integral; see eq. [10]) can then be written as

$$\delta\left(\frac{w}{r}v_r + \frac{d}{r}v_\phi - v_{\rm LOS}\right) = \frac{\delta\left[f(x,\, w) - \tilde{V}\right]}{(GM/r)^{1/2}(d/r)}, \tag{B2}$$

where

$$v_r = (GM/r)^{1/2}\,\tilde{v}_r, \quad v_\phi = (GM/r)^{1/2}\tilde{v}_\phi, \tag{B3}$$

$$\tilde{v}_r(x) = \left[\frac{1-x}{x}(2\beta - 1 + x)\right]^{1/2}, \tag{B4}$$

$$\tilde{v}_\phi(x) = x^{1/2}, \tag{B5}$$

$$\tilde{V} = \tilde{V}(w) = \frac{v_{\rm LOS}}{(GM/r)^{1/2}}\left(\frac{r}{d}\right) = \frac{v_{\rm LOS}}{v_{\rm orb}(d)}\left(\frac{r}{d}\right)^{3/2}. \tag{B6}$$

After the integration over x with use of the delta function, the only possible source of the singularity in the remaining integral over w is the denominator

$$\left|\tilde{v}_r(x)\frac{\partial f(x,\, w)}{\partial x}\right|, \tag{B7}$$

where $x = x(w,\, v_{\rm LOS})$ are the roots of $f(x,\, w) = \tilde{V}$. This denominator vanishes at the values of $w = w^*$ corresponding to zeros of $\partial f/\partial x$. The corresponding singularities are, however, of the form $1/(w-w^*)^{1/2}$ and so are integrable.

To see this, consider the vicinity of the $\partial f/\partial x = 0$ point that occurs at $x = \bar{x}$. From the form of $f(x,\, w)$ near the extremum

$$f(x,\, w) = \bar{f}(w) + \bar{g}(w)[x - \bar{x}(w)]^2, \tag{B8}$$

we find that the roots of $f(x,\, w) = \tilde{V}$ behave as $x - \bar{x}(w) = \pm\{[\tilde{V}(w) - \bar{f}(w)]/\bar{g}(w)\}^{1/2}$. The denominator given by equation (B7) is proportional to

$$2\bar{g}(w)[x - \bar{x}(w)] \propto \left[\tilde{V}(w) - \bar{f}(w)\right]^{1/2}. \tag{B9}$$

Suppose that as $w \to w^*$ the roots approach the point x^* at which $\partial f/\partial x = 0$ [this requires that $v_{\rm LOS}$ has a specific value, such that $f(x^*, w^*) = \tilde{V}(w^*)$ holds]. Expanding in powers of $(w - w^*)$,

$$\tilde{V}(w) = V^* + h(w - w^*), \tag{B10}$$

$$\bar{f}(w) = f^* + c(w - w^*), \tag{B11}$$

and using $\bar{x}(w^*) = x^*$, $f^* = V^*$, we find that the denominator indeed behaves as $(w - w^*)^{1/2}$. The validity of the expansions used above follows from the explicit form of $f(x, w)$ and $\tilde{V}(w)$.

The singularity of the w integral for $dN/dv_{\rm LOS}$ results from the presence of the factor $\tilde{v}_r$ in the denominator. This factor vanishes as $x \to 1$: $\tilde{v}_r \propto (1 - x)^{1/2}$. As a consequence, it is possible for the denominator to vanish at a point with $\partial f/\partial x$ nonzero. Near $x = 1$ the denominator $|\tilde{v}_r df/dx|$ has the form $|-(w/d)\beta + \tilde{v}_r/\tilde{v}_\phi|$, or equivalently $|-(w/d)\beta + [2\beta(1 - x)]^{1/2}|$. In the limit $x \to 1$, $f \to (w/d)[(2\beta)(1 - x)]^{1/2} + 1$, so that the equation for the roots becomes $[(2\beta)(1 - x)]^{1/2} = \tilde{V}(w) - 1$. As $w \to 0$ this has a solution provided that $v_{\rm LOS} = v_{\rm orb}(d)$: then $\tilde{V} = (r/d)^{3/2} = (1 + w^2/d^2)^{3/4}$. It follows that $[(2\beta)(1 - x)]^{1/2} \to \frac{3}{4}(w^2/d^2)$. The denominator then vanishes as w in the $w \to 0$ limit and there is a singularity.

APPENDIX C

TOY MODEL

To illustrate further how the logarithmic singularity in the integral for $dN/dv_{\rm LOS}$ arises, we introduce a simplified model, defined by replacing equation (B4) by

$$\tilde{v}_r(x) \approx (2\beta)^{1/2}(1 - x)^{1/2} \tag{C1}$$

(note that this model can be used to describe the behavior of the integral discussed in Appendix B in the limit $x \to 1$, relevant for the singularity). The roots $x(w, V_{\rm LOS})$ of the argument of the delta function, which can be written as

$$\tilde{V} = (w/d)\tilde{v}_r(x) + \tilde{v}_\phi(x), \tag{C2}$$

can then be easily found [it is a quadratic equation in $y \equiv (x)^{1/2}$], and their dependence on w and $V_{\rm LOS}$ followed. We have denoted

$$\tilde{V} \equiv \frac{V_{\rm LOS}}{v_{\rm orb}(d)}\left(\frac{r}{d}\right)^{3/2}, \tag{C3}$$

where $v_{\rm orb}(d) \equiv (GM/d)^{1/2}$ is the orbital speed at the distance d. The singularity of the integral over w, after the x integration is performed by use of the delta function, arises from the zero of

$$\tilde{v}_r \frac{d}{dx}\left(\frac{w}{d}\tilde{v}_r + \tilde{v}_\phi\right) = \frac{(2\beta)^{1/2}}{2}\left[\frac{w}{d}(2\beta)^{1/2} - \left(\frac{1 - x}{x}\right)^{1/2}\right]. \tag{C4}$$

It is convenient to assume that $\beta \gg 1$. Since the inner cutoff in the disk radius implies that $x > r_{\rm min}/r$, the above expression can only vanish at small enough w. It is then possible to omit the w dependence of $\tilde{V}$.

Denote $u \equiv (w/d)(2\beta)^{1/2}$. Using the explicit expressions for the roots $x(w/d, V_{\rm LOS})$ of equation (C2), one can rewrite the expression in the square brackets in equation (C4) as

$$\frac{w}{d}(2\beta)^{1/2}\frac{1}{x^{1/2}}\left(u^2 + 1 - \tilde{V}^2\right)^{1/2}. \tag{C5}$$

The integration region over w is, for $\tilde{V} \geq 1$, given by $(\tilde{V}^2 - 1)^{1/2} < u < \infty$ [of which the region $(\tilde{V}^2 - 1)^{1/2} < u < \tilde{V}$ corresponds to two roots of eq. (B2)], and, for $\tilde{V} < 1$, by $-\infty < u < \tilde{V}$ (one root only). Consider the case $\tilde{V} \geq 1$. The integral has the form

$$\begin{aligned}\frac{dN}{dV_{\rm LOS}} &\propto \int_{(\tilde{V}^2-1)^{1/2}} \frac{du}{\left(u^2 - \tilde{V}^2 + 1\right)^{1/2}}(\ldots) \\ &\propto \log\left[\left(\tilde{V}^2 - 1\right)^{1/2}\right] + \ldots,\end{aligned} \tag{C6}$$

leading to the logarithmic singularity as $\tilde{V} \to 1$ from above; that is, as $V_{\rm LOS} \to v_{\rm orb}(d)$. For $\tilde{V} \to 1$ from below, the logarithmic singularity arises from the $u = 0$ point inside the $-\infty < u < \tilde{V}$ integration region.

REFERENCES

Artymowicz, P. 1997, Annu. Rev. Earth Planet. Sci., 25, 175
Artymowicz, P., & Clampin, M. 1997, ApJ, 490, 863
Augereau, J. C., & Beust, H. 2006, A&A, 455, 987
Augereau, J. C., Nelson, R. P., Lagrange, A. M., Papaloizou, J. C. B., & Mouillet, D. 2001, A&A, 370, 447
Backman, D. E., & Paresce, F. 1993, in Protostars and Planets III, ed. E. H. Levy & J. I. Lunine (Tucson: Univ. Arizona Press), 1253
Beust, H., Lagrange, A.-M., Crawford, I. A., Goudard, C., Spyromilio, J., & Vidal-Madjar, A. 1998, A&A, 338, 1015
Beust, H., Lagrange, A.-M., Plazy, F., & Mouillet, D. 1996, A&A, 310, 181
Beust, H., & Morbidelli, A. 2000, Icarus, 143, 170
Bouret, J. C., & Deleuil, M. 2003, in The Future of Cool-Star Astrophysics: 12th Cambridge Workshop on Cool Stars, Stellar Systems, and the Sun, ed. A. Brown, G. M. Harper, & T. R. Ayres (Univ. Colorado), 710
Brandeker, A., Liseau, R., Olofsson, G., & Fridlund, M. 2004, A&A, 413, 681
Ferlet, R., Vidal-Madjar, A., & Hobbs, L. M. 1987, A&A, 185, 267
Fernández, R., Brandeker, A., & Wu, Y. 2006, ApJ, 643, 509
Grigorieva, A., Artymowicz, P., & Thébault, Ph. 2007, A&A, 461, 537
Hobbs, L. M., Vidal-Madjar, A., Ferlet, R., Albert, C. E., & Gry, C. 1985, ApJ, 293, L29
Hornung, K., & Kissel, J. 1994, A&A, 291, 324
Hornung, K., Malama, Y. G., & Kestenbohm, K. S. 2000, Ap&SS, 274, 355
Kalas, P., Graham, J. R., & Clampin, M. 2005, Nature, 435, 1067
Köhler, M., & Mann, I. 2002, in Asteroids, Comets, Meteorites 2002, ed. B. Wambein (Noordwijk: ESA), 771
Krivov, A. V., Mann, I., & Krivova, N. A. 2000, A&A, 362, 1127
Lagrange, A. M., Vidal-Madjar, A., Deleuil, M., Emerich, C., Beust, H., & Ferlet, R. 1995, A&A, 296, 499
Lagrange, A. M., et al. 1998, A&A, 330, 1091
Lecavelier des Etangs, A., et al. 2001, Nature, 412, 706
Li, A., & Greenberg, J. M. 1998, A&A, 331, 291
Liseau, R. 2003, in Proceedings of the Conference on Towards Other Earths: DARWIN/TPF and the Search for Extrasolar Terrestrial Planets, ed. M. Fridlund & T. Henning (ESA SP-539; Noordwijk: ESA), 135
Liseau, R., & Artymowicz, P. 1998, A&A, 334, 935
Mann, I., & Czechowski, A. 2005, ApJ, 621, L73
Mann, I., Koehler, M., Kimura, H., Czechowski, A., & Minato, T. 2006, A&A Rev., 13, 159
Mann, I., Murad, E., & Czechowski, A. 2007, Planet. Space Sci., in press
Marsh, K. A., Silverstone, M. D., Becklin, E. E., Koerner, D. W., Werner, M. W., Weinberger, A. J., & Ressler, M. E. 2002, ApJ, 573, 425
Minato, T., Köhler, M., Kimura, H., Mann, I., & Yamamoto, T. 2006, A&A, 452, 701
Mukai, T., & Schwehm, G. 1981, A&A, 95, 373
Nakamura, A. M., Fujiwara, A., & Kadono, T. 1994, Planet. Space Sci., 42, 1043
Okamoto, Y. K., et al. 2004, Nature, 431, 660
Olofsson, G., Liseau, R., & Brandeker, A. 2001, ApJ, 563, L77
Plavchan, P., Jura, M., & Lipscy, S. J. 2005, ApJ, 631, 1161
Roberge, A., Feldman, P. D., Weiberger, A. J., Deleuil, M., & Bouret, J.-C. 2006, Nature, 441, 724
Su, K. Y. L., et al. 2005, ApJ, 628, 487
Sugita, S., Schultz, P. H., & Adams, M. A. 1997, in 28th Annual Lunar and Planetary Science Conference, 1393
Takeuchi, T., & Artymowicz, P. 2001, ApJ, 557, 990
Takeuchi, T., Clarke, C. J., & Lin, D. N. C. 2005, ApJ, 627, 286
Tamura, M., Fugukawa, M., Kimura, H., Yamamoto, T., Suto, H., & Abe, L. 2006, ApJ, 641, 1172
Thébault, P., & Augereau, J. C. 2005, A&A, 437, 141
Tielens, A. G. G. M., McKee, C. F., Seab, C. G., & Hollenbach, D. J. 1994, ApJ, 431, 321
Tomeoka, K., Kiriyama, K., Nakamura, K., & Yamahana, Y. 2003, Nature, 423, 60
Vidal-Madjar, A., Lecavelier des Etangs, A., & Ferlet, R. 1998, Planet. Space Sci., 46, 629
Wahhaj, Z., Koerner, D. W., Ressler, M. E., Werner, M. W., Backman, D. E., & Sargent, A. I. 2003, ApJ, 584, L27